ChemPubSoc Europe

DOI: 10.1002/ejic.201801182

EurJIC European Journal of Inorganic Chemistry

Full Paper

Rare-Earth Phosphates

Crystallization Pathways of Cerium(IV) Phosphates Under Hydrothermal Conditions: A Search for New Phases with a Tunnel Structure

Taisiya O. Shekunova,[a,b] Sergey Ya. Istomin,[b] Andrey V. Mironov,[b] Alexander E. Baranchikov,[a,b] Alexey D. Yapryntsev,[a] Arsen A. Galstyan,[b] Nikolay P. Simonenko,[a] Andrey A. Gippius,[b,c] Sergey V. Zhurenko,[b,c] Tatyana B. Shatalova,[b] Lyudmila S. Skogareva,[a] and Vladimir K. Ivanov*[a,d]

Abstract: Hydrothermal crystallization pathways of amorphous ceric phosphate gels were found to be determined by the ammonia concentration in a reaction medium. This allows for highly selective hydrothermal synthesis of various finely crystalline ceric phosphates, including $Ce(PO_4)(HPO_4)_{0.5}(H_2O)_{0.5}$, $(NH_4)_2Ce(PO_4)_2(H_2O)$, and previously unknown $NH_4Ce_2(PO_4)_3$. The structure of the latter compound was solved from powder X-ray diffraction data. It appeared to be isostructural to ammonium thorium phosphate, $NH_4Th_2(PO_4)_3$; in this crystal structure, large channels (5.07 × 3.79 Å) located along the *c*-axis are occupied by NH_4^+ ions.

Introduction

Crystalline rare-earth phosphates are widely used in high-tech industrial applications such as for optical materials, heat-resistant ceramics, ion-exchange materials, luminophores and as radioactive waste sorbents.[1–7] Cerium phosphates are of particular interest since they can contain cerium ions in both +3 and +4 oxidation states. The crystallographic data and properties of cerium(III) phosphates – monazite ($P2_1/n$) and rhabdophane ($P6_222$) – have been thoroughly studied.[8–10] Surprisingly, information on cerium(IV) phosphates is extremely scarce, despite their long history since the middle of the 20th century[11–13] and rich ceric coordination chemistry.[14]

Recently, Nazarali et al. managed to obtain and characterize ceric hydrogen orthophosphate – $Ce(PO_4)(HPO_4)_{0.5}(H_2O)_{0.5}$.[15] This compound was synthesized by hydrothermal treatment of ceric phosphate acid solution, and its structure was found to contain dense double layers of $[Ce(PO_4)^+]_n$. A compound with an identical structure and the assigned composition $Ce_2(PO_4)_2HPO_4{\cdot}H_2O$ was synthesized earlier by Brandel et al.,[16] using hydrothermal treatment of solutions containing $(NH_4)_2Ce(NO_3)_6$, H_3PO_4 and HNO_3. Nazarali et al. also synthesized another ceric hydrogen orthophosphate, $Ce(PO_4)_{1.5}(H_2O)(H_3O)_{0.5}(H_2O)_{0.5}$, via the hydrothermal method.[17] The structure of the latter contains a negatively charged three-dimensional framework, with eight-coordinated Ce^{IV} polyhedra connected through PO_4^{3-} tetrahedra and tunnels containing water molecules and charge-compensating H_3O^+ cations. Hydronium cations can be substituted with alkali metal cations by an ion exchange, which proceeds most efficiently for small cations ($Li^+ > Na^+ = K^+ > Rb^+ > Cs^+$) due to the steric effect.[18]

In addition to ceric hydrogen orthophosphates, double orthophosphates are also known. Orlova et al.[19] obtained a number of compounds with the composition $A_{0.5}Ce_2(PO_4)_3$, $ACe(PO_4)_2$, $ARCe(PO_4)_3$ (A = Mg–Ba, Cd; R = Nd, Gd), which are isostructural to monazite and considered as promising matrices for the immobilization of radioactive wastes. Xu et al. obtained two crystalline double orthophosphates of cerium and single-charged cations: $K_2Ce(PO_4)_2{\cdot}H_2O$[20] and $(NH_4)_2Ce(PO_4)_2{\cdot}H_2O$[21] via hydrothermal treatment of hydrated CeO_2 in a partially neutralized phosphoric acid solution. The authors demonstrated that the obtained compounds had a pronounced proton conductivity, and, at elevated temperatures, a potassium ions conductivity.

Salvado et al.[22] synthesized $(NH_4)_2Ce(PO_4)_2{\cdot}H_2O$ by a similar hydrothermal method using CeO_2, $CO(NH_2)_2$ and H_3PO_4 as starting materials, and revised the structural data presented by Xu et al. According to Salvado et al.,[22] the structure of this compound comprises eight-coordinated cerium atoms interconnected with phosphate groups and contains tunnels of various sizes with ammonium ions and water molecules.

The synthesis and structure of another double ceric orthophosphate, $Na_{10}Ce_2(PO_4)_6$, have been reported by Lai et al.[23]

[a] *Kurnakov Institute of General and Inorganic Chemistry of the Russian Academy of Sciences, Moscow, Russia*
E-mail: van@igic.ras.ru
[b] *Lomonosov Moscow State University, Moscow, Russia*
[c] *Lebedev Physical Institute of the Russian Academy of Sciences, 119991, Moscow, Russia*
[d] *National Research Tomsk State University, Tomsk, Russia*
Supporting information and ORCID(s) from the author(s) for this article are available on the WWW under https://doi.org/10.1002/ejic.201801182.

This compound was obtained by high-temperature hydrothermal treatment of NaF, CeO_2, NaOH and NaH_2PO_4. In the $Na_{10}Ce_2(PO_4)_6$ structure, each Ce cation is connected to three others through phosphate groups, forming a three-dimensional network with intersecting channels. Sodium ions are located inside these channels.

Bevara et al.[24] synthesized a crystalline double ceric orthophosphate, $K_2Ce(PO_4)_2$, by a solid-state reaction between stoichiometric amounts of KPO_3 (or KH_2PO_4) and CeO_2. They showed that $K_2Ce(PO_4)_2$ has a structure containing one-dimensional channels formed by eight-coordinated Ce^{IV} and PO_4 tetrahedra with potassium cations inside the channels.

More complex ceric orthophosphates may also have a similar structure, with channels containing potassium cations. For instance, Ogorodnik et al.[25] synthesized ternary orthophosphate $K_4CeZr(PO_4)_4$ by solid-phase synthesis using ZrF_4, CeF_3, KPO_3 and $K_4P_2O_7$ as initial reagents.

Note that almost all of the abovementioned ceric orthophosphates have a three-dimensional framework containing empty or filled tunnels. This feature explains the ion exchangeability and sorption properties of these compounds.

However, the data on ceric orthophosphates are rather limited, since they tend to form amorphous phases when synthesized from aqueous solutions.[26–29] High temperature treatment, in turn, eventually results in the decomposition of Ce^{IV} compounds, with the formation of Ce^{III} species.[16] Apparently, the only rational pathway for the preparation of crystalline ceric orthophosphates is a mild hydrothermal treatment. Under certain conditions, hydrothermal treatment allows for the synthesis of different crystalline phases simply by adjusting the composition of hydrothermal media. Previously, we have shown that hydrothermal treatment of ceric phosphate gels leads to the formation of $Ce(PO_4)(HPO_4)_{0.5}(H_2O)_{0.5}$ or rhabdophane, depending on the synthetic conditions.[30]

In this paper, we have explored ceric orthophosphates' crystallization pathways under hydrothermal conditions in the presence of ammonium hydroxide. This approach allowed us to selectively synthesize not only previously reported $Ce(PO_4)(HPO_4)_{0.5}(H_2O)_{0.5}$ and $(NH_4)_2Ce(PO_4)_2(H_2O)$ phases, but also a novel ceric orthophosphate, $NH_4Ce_2(PO_4)_3$.

Results and Discussion

According to powder X-ray diffraction data, mixing a cerium-containing phosphate solution (concentration 0.1 M) with 0.01 M ammonia solution, and subsequent hydrothermal treatment of the gel formed, resulted in $Ce(PO_4)(HPO_4)_{0.5}(H_2O)_{0.5}$ phase. A similar product was formed upon hydrothermal treatment of cerium-containing phosphate gels obtained by mixing a cerium-containing phosphate solution with pure water.[30] When more concentrated ammonia solutions (0.1–3 M) were used, the phase composition of the hydrothermal treatment products changed (see Figure 1, Fig. S1–S3). In particular, the use of NH_4OH in concentrations above 2 M resulted in the formation of $(NH_4)_2Ce(PO_4)_2(H_2O)$ phase, as described by Salvado et al.[22] In turn, the use of intermediate concentrations of NH_4OH (0.1–2 M) led to the crystallization of a phase which is absent in the ICDD PDF database.

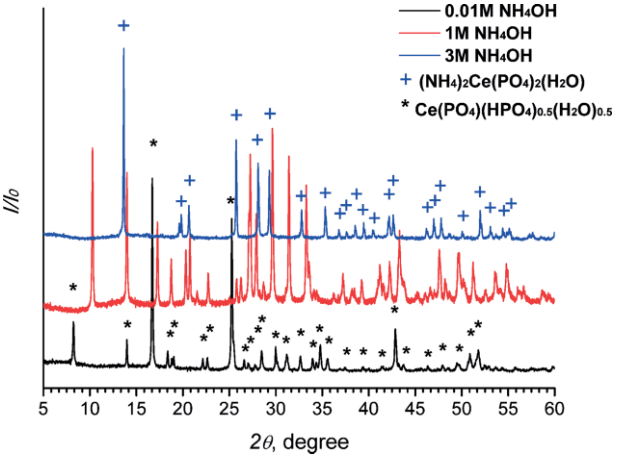

Figure 1. Powder X-ray diffraction patterns of crystalline products obtained by hydrothermal treatment of cerium-containing phosphate gels formed upon the addition of NH_4OH with different concentrations: 0.01 M – all peaks correspond to the $Ce(PO_4)(HPO_4)_{0.5}(H_2O)_{0.5}$ phase (marked with *), 1 M – all peaks correspond to the new phase, 3 M – all peaks correspond to the $(NH_4)_2Ce(PO_4)_2(H_2O)$ phase (marked with +).

The powder XRD pattern of the sample obtained upon addition of 1 M NH_4OH was fully indexed using TOPAS 4.2 software in monoclinic space group *C*2/*c*, with the unit cell parameters a = 17.4810(6) Å, b = 6.7716(2) Å, c = 7.9987(3) Å, β = 102.887(2)°. The crystal structure was solved using the direct space Monte Carlo simulation by FOX software package.[31] The identification of the crystal structure was simplified by the fact that it contains PO_4 groups and heavy Ce cations. At the initial stage of the crystal structure solution, two crystallographically independent PO_4 groups and one Ce atom were isolated. They were responsible for *ca.* 90% of the scattering power in the crystal structure. At the final stage, N atoms were located, and the ammonia group was refined as a rigid body with a fixed geometric configuration. The final Rietveld refinement of the crystal structure was performed using JANA2000 software.[32] The composition of the novel phase corresponded to the chemical formula $NH_4Ce_2(PO_4)_3$. The chemical composition of the phase was confirmed by EDX analysis, which showed that the P/Ce ratio was 1.5, and by CHN-analysis, which resulted in nitrogen content of 2.0 wt. % (calculated 2.4 wt. %) and hydrogen content of 1.1 wt. % (calculated 0.7 wt. %). Crystal data, refined atomic coordinates, and displacement parameters are given in Table S1, and selected interatomic distances are presented in Table S2. Observed and calculated PXRD profiles are shown in Figure 2. The crystal structure of $NH_4Ce_2(PO_4)_3$ is shown in Figure 3. In this crystal structure, each Ce atom is coordinated by 9 oxygen atoms belonging to PO_4 tetrahedra. Large channels (5.07 Å along *a*-axis and 3.79 Å along *b*-axis) occupied by NH_4^+ groups are located along the *c*-axis of the crystal structure.

Static ^{31}P NMR spectrum of the $NH_4Ce_2(PO_4)_3$ powder sample measured at room temperature is presented in Figure 4. The NMR peak is relatively narrow (FWHM = 7.74 kHz) and slightly asymmetric with a more elongated left shoulder. As depicted in Figure 4, it was successfully fitted by two Lorentzian lines with almost equal width and the peak positions of –27(5) ppm

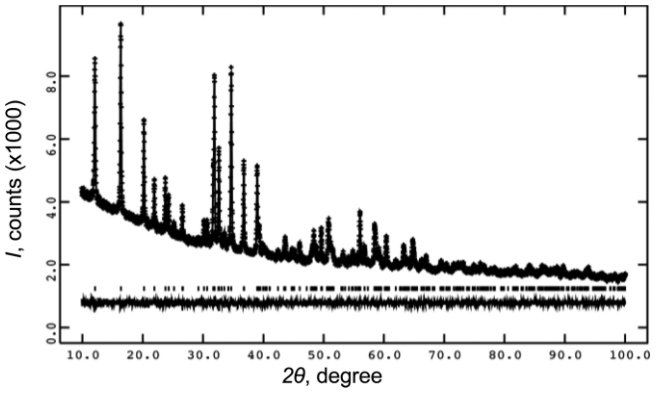

Figure 2. Observed and calculated PXRD profiles of $NH_4Ce_2(PO_4)_3$ and the difference between them. The vertical ticks indicate the reflection positions.

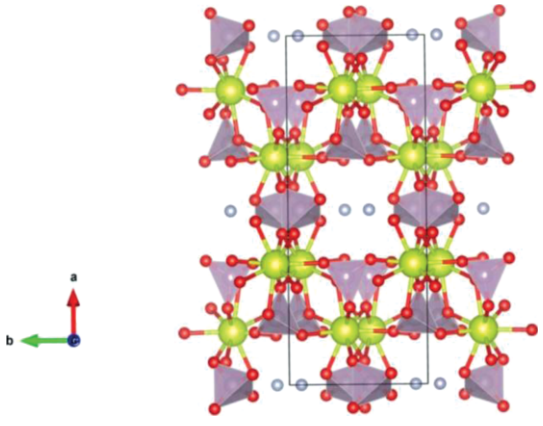

Figure 3. Crystal structure of $NH_4Ce_2(PO_4)_3$ viewed along the c-axis. Yellow circles denote Ce atoms, N atoms are shown in gray, O atoms are presented as red circles, P atoms are located in PO_4 tetrahedra (shown in violet color).

and +10(5) ppm for Lorentz-I and Lorentz-II lines, respectively. The ratio of integral intensities of these two lines (1:2.18) was found to be rather close to the multiplicity ratio 1:2 of two inequivalent phosphorus crystallographic positions in the $NH_4Ce_2(PO_4)_3$ crystal structure (see Table S1). Consequently, the obtained ^{31}P NMR results supported well the $NH_4Ce_2(PO_4)_3$ structural refinement.

The new compound obtained by us is a representative of a wider class of double phosphates of the general composition $M^IM^{IV}_2(PO_4)_3$.[33] Despite the significant number of such compounds, the conditions for their formation are still under study and discussion. This is probably due to the fact that $M^IM^{IV}_2(PO_4)_3$ (M^I = Li–Cs) phases can be of different structural types, depending on the nature of M^{IV}. For instance, the compounds $M^IM^{IV}_2(PO_4)_3$ with M^{IV} = Ce have the monazite structure (space group $P2_1/n$), while the compounds with M^{IV} = Ge, Sn, Ti, Zr, Hf or actinides (Th, U, Pu) belong to NASICON-type [NASICON refers to **Na S**uper **I**onic **Con**ductors, the abbreviation denotes a special class of $M^IM^{IV}_2(PO_4)_3$ compounds] trigonal or monoclinic systems.[34–35] With this in mind, the absence of information about $M^ICe^{IV}_2(PO_4)_3$ phases isostructural to double actinide (e.g. thorium) orthophosphates is surprising, since cerium(IV) and thorium(IV) form isostructural phosphates[36–38] due to their close ionic radii (0.97 and 1.05 Å for Ce and Th

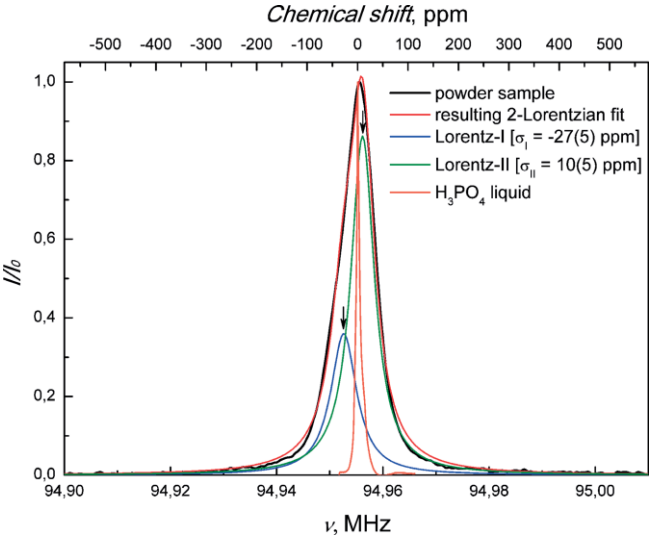

Figure 4. ^{31}P NMR spectrum of the $NH_4Ce_2(PO_4)_3$ powder measured at room temperature.

with coordination number 8, respectively[39]). Our findings demonstrate the first example of a cerium phosphate [$NH_4Ce_2(PO_4)_3$] isostructural to $M^IR^{IV}_2(PO_4)_3$ (R = actinide). For example, recently reported thorium-ammonium phosphate, $NH_4Th_2(PO_4)_3$ (monoclinic system, space group $C2/c$, unit cell parameters: a = 17.7238(5) Å, b = 6.90676(12) Å, c = 8.15603(32) Å, β = 102.1047(26)°[40]) possesses the same structure. The $NH_4Ce_2(PO_4)_3$ phase is also worthy of note, as only a few $M^IM^{IV}_2(PO_4)_3$ phases are known where $M^I = NH_4^+$. To the best of our knowledge, the known representatives of such phases include the ammonium-zirconium phosphates described by Clearfield et al. in 1984[41] and the ammonium-thorium phosphates obtained by Salvado et al. in 2008.[40,42] At the same time, similar potassium containing compounds have been known since 1889,[43] while potassium and ammonium have very close ionic radii (1.51[39] and 1.54 Å[44] for coordination number 8, respectively).

Thus, we proposed a synthetic technique that made it possible to produce three different ceric orthophosphates, which is quite unusual. Apparently, the formation of ceric hydrogen orthophosphate $Ce(PO_4)(HPO_4)_{0.5}(H_2O)_{0.5}$ occurs when there are practically no ammonium cations in the system (molar ratio H_3PO_4/NH_4OH exceeds 200). The gradual increase in ammonia concentration (up to molar ratio $H_3PO_4/NH_4OH \approx 20$ and lower) results in ceric ammonium phosphate formation having Ce/P ratios of 1.5 and 2.0 ($NH_4Ce_2(PO_4)_3$ and $(NH_4)_2Ce(PO_4)_2(H_2O)$, respectively). The exact reason for the formation of different crystalline phases by variation of the ammonia concentration is not clear but this effect is obviously related in some way to the different complexation of Ce^{IV} ions by phosphate ions in the solutions. The lack of data on the composition and properties of ceric phosphate complexes hinders the explanation of the formation of different phosphate phases.

$Ce(PO_4)(HPO_4)_{0.5}(H_2O)_{0.5}$, $NH_4Ce_2(PO_4)_3$ and $(NH_4)_2Ce(PO_4)_2(H_2O)$ were further characterized by IR spectroscopy, SEM and thermal analysis. Figure 5 shows the IR spectra of $Ce(PO_4)(HPO_4)_{0.5}(H_2O)_{0.5}$, $NH_4Ce_2(PO_4)_3$ and $(NH_4)_2Ce(PO_4)_2$-

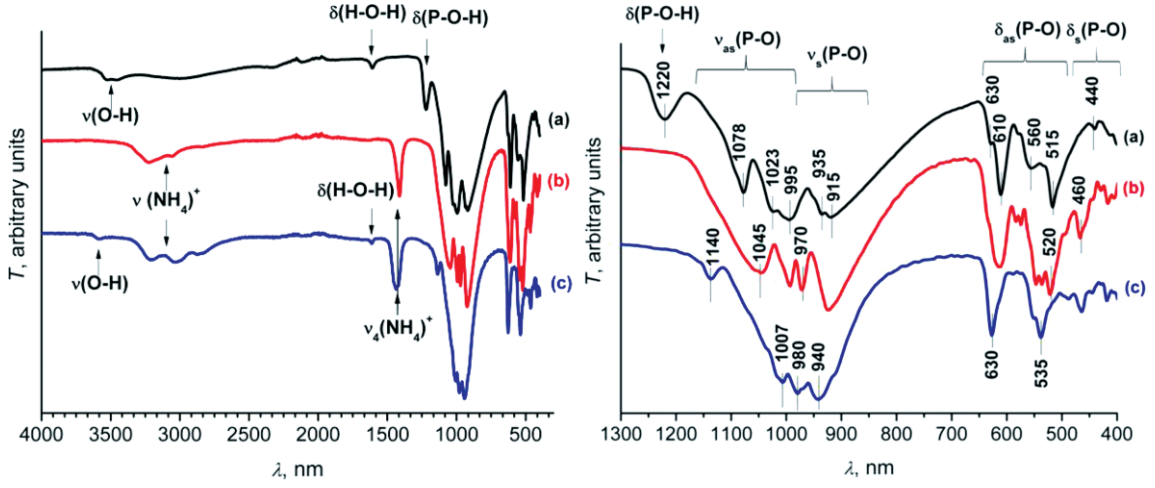

Figure 5. The survey IR spectrum, left (300–4000 cm^{-1}), and its fragment, right (400–1300 cm^{-1}): $Ce(PO_4)(HPO_4)_{0.5}(H_2O)_{0.5}$ (a), $NH_4Ce_2(PO_4)_3$ (b), $(NH_4)_2Ce(PO_4)_2(H_2O)$ (c).

(H_2O) phases. One can see that the general pattern of the IR spectra of these compounds is almost the same and is characteristic for rare-earth phosphates,[45–48] although there are some differences. For example, in the IR spectra of $NH_4Ce_2(PO_4)_3$ and $(NH_4)_2Ce(PO_4)_2(H_2O)$, in contrast to the IR spectrum of $Ce(PO_4)(HPO_4)_{0.5}(H_2O)_{0.5}$, absorption bands at 2800–3300 cm^{-1} (br) and 1430 cm^{-1} (s) are observed, which are related to the stretching and bending vibrations of the NH_4^+ ion.[49–51]

As expected, the IR spectra of $(NH_4)_2Ce(PO_4)_2(H_2O)$ and $Ce(PO_4)(HPO_4)_{0.5}(H_2O)_{0.5}$ contained the absorption bands of water molecules, corresponding to O–H-bond stretching (3550–3660 cm^{-1}, br) and H–O–H bending vibrations (1600 cm^{-1}, w). The splitting of the ν(OH) band in the IR spectrum of $Ce(PO_4)(HPO_4)_{0.5}(H_2O)_{0.5}$ is presumably due to the presence of two types of OH groups in the compound (H_2O molecules and HPO_4^{2-} anions).[52] The absence of water molecules' absorption bands and the presence of NH_4^+ ion absorption bands also validate the composition of the $NH_4Ce_2(PO_4)_3$ phase.

The absorption maximum at 1220 cm^{-1} (m), which is present only in the IR spectrum of $Ce(PO_4)(HPO_4)_{0.5}(H_2O)_{0.5}$, apparently refers to P–O–H bending vibrations[16] (see Figure 5). The absorption bands at 1180–990 cm^{-1} refer to the asymmetric stretching vibrations ν_3, and the bands at 980–900 cm^{-1} to the symmetric stretching vibrations ν_1 of P–O bonds in phosphate groups. Absorption bands at 650–440 cm^{-1} correspond to δ(O–P–O), and those at 440 cm^{-1} correspond to symmetric ν_2 vibrations (see Figure 5).[53–54]

The splitting of the IR-absorption bands in the region corresponding to the PO_4^{3-} ion oscillations (1200–900 cm^{-1} and 500–600 cm^{-1}) suggests the conclusion that the PO_4 groups in all the phases are coordinated with cerium atoms, while the different splitting degree is possibly related to the different denticity of PO_4 groups and/or distortions due to their coordination by large, multicharged cations.[55]

According to SEM data, the $Ce(PO_4)(HPO_4)_{0.5}(H_2O)_{0.5}$ phase forms lamellar particles, the $NH_4Ce_2(PO_4)_3$ phase elongated microparticles and the $(NH_4)_2Ce(PO_4)_2(H_2O)$ phase truncated octahedral particles (see Figure 6).

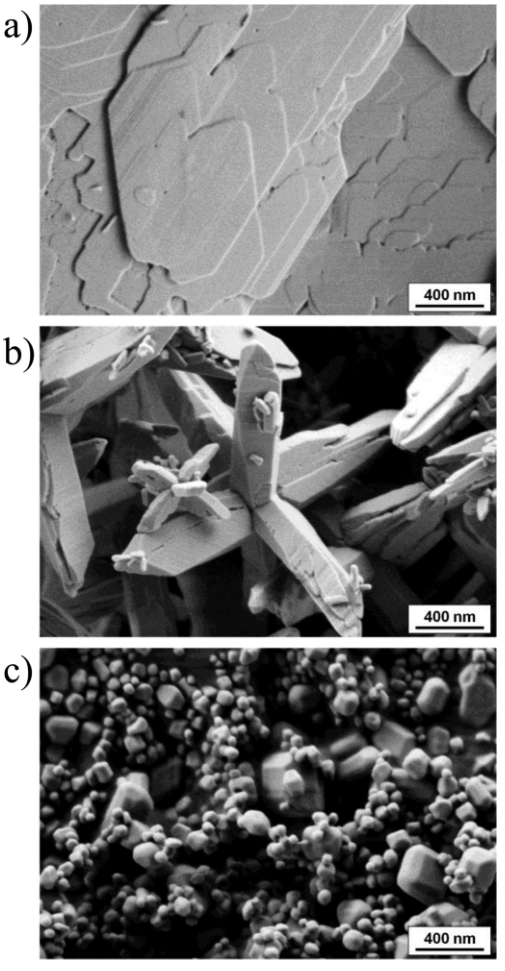

Figure 6. SEM images of (a) $Ce(PO_4)(HPO_4)_{0.5}(H_2O)_{0.5}$, (b) $NH_4Ce_2(PO_4)_3$ and (c) $(NH_4)_2Ce(PO_4)_2(H_2O)$.

Thermal analysis data for $(NH_4)_2Ce(PO_4)_2(H_2O)$, $Ce(PO_4)(HPO_4)_{0.5}(H_2O)_{0.5}$ and $NH_4Ce_2(PO_4)_3$ are presented in Figure S4 a,b and Figure 7, respectively. The thermal behavior of $(NH_4)_2Ce(PO_4)_2(H_2O)$ and $Ce(PO_4)(HPO_4)_{0.5}(H_2O)_{0.5}$ phases is in agreement with previously reported data.[16,22]

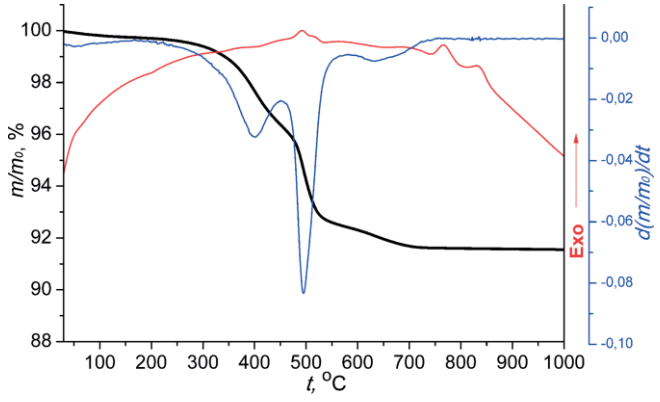

Figure 7. Results of thermal analysis of $NH_4Ce_2(PO_4)_3$ in air.

The thermal analysis of the new phase, $NH_4Ce_2(PO_4)_3$, revealed some interesting points. Particular attention was paid to the comparison of the thermal behavior of the isostructural $NH_4Ce_2(PO_4)_3$ and $NH_4Th_2(PO_4)_3$, since cerium, in contrast to thorium, can exist both in +3 and +4 oxidation states. According to our data, the thermal decomposition behavior of $NH_4Ce_2(PO_4)_3$ and $NH_4Th_2(PO_4)_3$ were completely different. The latter possessed extremely high thermal stability and decomposes almost in one stage above 700 °C to form β-$Th_4(PO_4)_4(P_2O_7)$.[40] In contrast, the thermal decomposition of $NH_4Ce_2(PO_4)_3$ began only at *ca.* 400 °C and occurred in several steps. Such a difference in the thermal stability of $NH_4Th_2(PO_4)_3$ and $NH_4Ce_2(PO_4)_3$ is most likely due to the changes in cerium oxidation state (see, for example [56–58]), that results in a complex and multistage $NH_4Ce_2(PO_4)_3$ decomposition.

Additional information on the thermal behavior of $NH_4Ce_2(PO_4)_3$ phase was obtained by mass-spectroscopy of the evolved gases. Surprisingly, we found that, even in Ar atmosphere at 250–600 °C, thermal decomposition was accompanied by the release of NO (m/z = 30) and H_2O (m/z = 18) (see Figure 8). We failed to detect reliably the presence of gaseous ammonia (e.g. m/z = 15) in the evolved gases. The formation of nitrogen monoxide under these conditions is unusual; however, we can suppose that ammonia, released during $NH_4Ce_2(PO_4)_3$ thermolysis, is oxidized to NO by ceric cations. Interestingly, the conversion of ammonia to NO was suggested by Clearfield et al. during thermolysis of $NH_4Zr_2(PO_4)_3$.[41] Such a reaction was believed to be of a catalytic nature, and to proceed due to the formation of strongly acidic sites upon $NH_4Zr_2(PO_4)_3$ decomposition. Oi et al. criticized Clearfield's supposition and noted that the oxidation of ammonia in the presence of $NH_4Zr_2(PO_4)_3$ requires not a superacid catalyst, but a redox active one (for example, platinum).[59] In our case, ceric cations might, for example, be a redox active species.

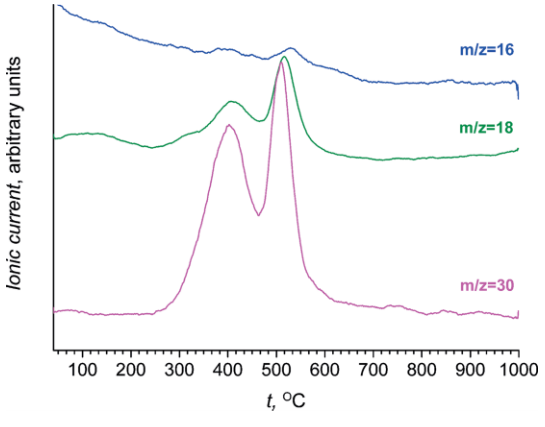

Figure 8. The temperature dependences of the ionic currents for $NH_4Ce_2(PO_4)_3$ in Ar atmosphere (m/z = 16, 18, 30).

The reduction of cerium +4 to +3 during the thermolysis of $NH_4Ce_2(PO_4)_3$ was confirmed by PXRD data. Upon the annealing of $NH_4Ce_2(PO_4)_3$ at 850 °C, the formation of $CePO_4$ (monazite, ICDD PDF 00–032–0199) was observed (see Figure S5).

The obtained data suggest that the thermal decomposition of ceric ammonium phosphate, $NH_4Ce_2(PO_4)_3$, up to 850 °C is a complex multistage process resulting in the formation of crystalline monazite and, apparently, a polyphosphate phase of an amorphous structure which cannot be reliably detected by means of X-ray diffraction.

Conclusions

In this paper, we have demonstrated that the hydrothermal treatment of amorphous ceric phosphates results in the selective formation of different crystalline products, depending on the amount of ammonia added to the reaction mixture: $Ce(PO_4)(HPO_4)_{0.5}(H_2O)_{0.5}$, $(NH_4)_2Ce(PO_4)_2(H_2O)$, or a novel phase, $NH_4Ce_2(PO_4)_3$. We solved the structure of $NH_4Ce_2(PO_4)_3$, and it was found to be isostructural to $NH_4Th_2(PO_4)_3$, containing a three-dimensional framework with large tunnels occupied by ammonium ions.

Experimental Section

Materials and Methods: The following materials were used as received, without further purification: $Ce(NO_3)_3{\cdot}6H_2O$ (99%, Aldrich #238538), orthophosphoric acid (85 wt. % aq, ρ = 1.689 g/cm^3, analytical grade, Khimmed Russia), aqueous ammonia (25 wt. %, extrapure grade, Khimmed Russia), distilled or deionised (18 MΩ) water.

The synthesis of the initial cerium-containing phosphoric acid solution was carried out according to a procedure reported earlier by us.[30] A sample of nanocrystalline (4–5 nm) cerium dioxide (0.100 g) obtained by precipitation from $Ce(NO_3)_3{\cdot}6H_2O$[60] was dissolved in concentrated orthophosphoric acid (5 mL) at 80 °C. The molar ratio of Ce/P was 1:126. After cooling the solution, 35 mL of aqueous ammonia solution (0.01–3 M concentration range) was added under vigorous stirring, so that the molar ratios of Ce/NH_4OH were from 1:0.6 to 1:180. The interaction of cerium-containing phosphate solution with the ammonia solution results in almost instant gelation. The reaction mixtures (≈ 40 mL) were placed in 100 mL Teflon autoclaves and subjected to hydrothermal treatment at 180 °C for 24 hours. After cooling the autoclaves, yellowish, slow-sedimenting precipitates were repeatedly washed using deionized water and dried at 60 °C.

Powder X-ray diffraction patterns were recorded with a Bruker D8 Advance diffractometer using Cu-$K_{\alpha1,2}$ radiation in the 2θ range 3–120°, at a 2θ step of 0.02° and a counting time of 0.3 s per step. The samples prepared to solve the structure were analyzed using a STOE STADI P powder diffractometer with a spinning sample in symmetric transmission mode (Co-$K_{\alpha1}$ radiation, λ = 1.78896 Å).

The microstructure (scanning electron microscopy, SEM) and the chemical composition (energy dispersive X-ray analysis, EDX) of the samples were analyzed on a Carl Zeiss NVision 40 high-resolution scanning electron microscope equipped with an Oxford Instruments X-MAX (80 mm^2) detector, operating at an accelerating voltage of 1–20 kV. SEM images were taken using an Everhart-Thornley detector (SE2) at 1 kV accelerating voltage.

Thermal analysis was performed on a TGA/DSC/DTA SDT Q-600 analyzer (TA Instruments), upon linear heating to 1000 °C (heating rate of 10 °C/min) in a 250 mL/min airflow.

The evolved gases were analyzed using a QMS 403C Aëolos quadrupole mass spectrometer (Netzsch, Germany) combined with a Netzsch STA 409 PC Luxx thermoanalytical system in Ar atmosphere at a heating rate of 10 °C/min.

The FTIR spectra of the samples were recorded on a Bruker ALPHA spectrometer, in a range of 400–4000 cm^{-1}, in attenuated total reflectance mode.

CHN-analysis was performed using a EuroVector EA3000 CHNS elemental analyzer.

^{31}P NMR spectrum of the $NH_4Ce_2(PO_4)_3$ sample was measured using self-built coherent pulsed NMR spectrometer at 5.509 T. The bore superconducting magnet possessed the magnetic field space homogeneity of about 5 ppm. The ^{31}P NMR spectrum was obtained by the Fourier transform of the FID signal after the $\pi/2$ pulse of 5 μs duration. Concentrated H_3PO_4 aqueous solution (≈ 85%) was used as a ^{31}P chemical shift reference sample. The ^{31}P NMR resonance frequency of H_3PO_4 measured using the spectrometer was 94.95523 MHz.

CCDC 1879687 for $NH_4Ce_2(PO_4)_3$ contains the supplementary crystallographic data for this paper. These data can be obtained free of charge from The Cambridge Crystallographic Data Centre.

Acknowledgments

The study was supported by Russian Foundation for Basic Research (RFBR 18-33-00275).

Keywords: Cerium · Hydrothermal synthesis · Gels · Synthesis design

[1] S. N. Achary, S. Bevara, A. K. Tyagi, *Coord. Chem. Rev.* **2017**, *340*, 266–297..
[2] Q. Li, V. W.-W. Yam, *Angew. Chem. Int. Ed.* **2007**, *46*, 3486–3489; *Angew. Chem.* **2007**, *119*, 3556–3559.
[3] M. R. Rafiuddin, A. P. Grosvenor, *Inorg. Chem.* **2016**, *55*, 9685–9696.
[4] S. Neumeier, Y. Arinicheva, Y. Ji, J. M. Heuser, P. M. Kowalski, P. Kegler, H. Schlenz, D. Bosbach, G. Deissmann, *Radiochim. Acta* **2017**, *105*, 961–984.
[5] H. Schlenz, S. Neumeier, A. Hirsch, L. Peters, & G. Roth in *Highlights in Applied Mineralogy* (Eds.: S. Heuss-Aßbichler, G. Amthauer, M. John), Walter de Gruyter GmbH, Berlin/Boston, **2018**, pp. 171–196.
[6] T. Anfimova, Q. Li, J. O. Jensen, N. J. Bjerrum, *Int. J. Electrochem. Sci.* **2014**, *9*, 2285–2300.
[7] W. Di, X. Wang, X. Ren, *Nanotechnology* **2010**, *21*, 075709–075714.
[8] G. Nagy, E. Draganits, *Mitt. Ges. Geol. Bergbaustud. Österr.* **1999**, *42*, 21–36.
[9] R. C. L. Mooney, *Acta Crystallogr.* **1950**, *3*, 337–340.
[10] Z.-G. Yan, Y.-W. Zhang, L.-P. You, R. Si, C.-H. Yan, *J. Cryst. Growth* **2004**, *262*, 408–411.
[11] G. Alberti, U. Constantino, F. D. Gregorio, P. Galli, E. Torracca, *J. Inorg. Nucl. Chem.* **1968**, *30*, 295–304.
[12] P. Barboux, R. Morineau, J. Livage, *Solid State Ionics* **1988**, *27*, 221–225.
[13] M. Casciola, U. Constantino, S. D'Amico, *Solid State Ionics* **1988**, *28*, 617–621.
[14] Y.-M. So, W.-H. Leung, *Coord. Chem. Rev.* **2017**, *340*, 172–197.
[15] M. Nazaraly, G. Wallez, C. Chaneac, E. Tronc, F. Ribot, M. Quarton, J.-P. Jolivet, *Angew. Chem. Int. Ed.* **2005**, *44*, 5691–5694; *Angew. Chem.* **2005**, *117*, 5837–5840.
[16] V. Brandel, N. Clavier, N. Dacheux, *J. Solid State Chem.* **2005**, *178*, 1054–1063.
[17] M. Nazaraly, C. Chaneac, F. Ribot, G. Wallez, M. Quarton, J.-P. Jolivet, *J. Phys. Chem. Solids* **2007**, *68*, 795–798.
[18] M. Nazaraly, M. Quarton, G. Wallez, C. Chaneac, F. Ribot, J.-P. Jolivet, *Solid State Sci.* **2007**, *9*, 672–677.
[19] A. I. Orlova, D. B. Kitaev, *Radiochemistry* **2005**, *47*, 14–30.
[20] Y. Xu, S. Feng, W. Pang, *Mater. Lett.* **1996**, *28*, 499–502.
[21] Y. Xu, S. Feng, W. Pang, G. Pang, *Chem. Commun.* **1996**, *0*, 1305–1306.
[22] M. Salvado, P. Pertierra, C. Trobajo, J. Garcıa, *J. Am. Chem. Soc.* **2007**, *129*, 10970–10971.
[23] Y.-H. Lai, Y.-C. Chang, T.-F. Wong, W.-J. Tai, W.-J. Chang, K.-H. Lii, *Inorg. Chem.* **2013**, *52*, 13639–13643.
[24] S. Bevara, S. N. Achary, S. J. Patwe, A. K. Sinha, A. K. Tyagi, *Dalton Trans.* **2016**, *45*, 980–991.
[25] I. V. Ogorodnyk, I. V. Zatovsky, V. N. Baumer, N. S. Slobodyanik, O. V. Shishkin, *Acta Crystallogr., Sect. C: Cryst. Struct. Commun.* **2006**, *62*, i100–i102.
[26] W. N. Hartley, *J. Chem. Soc.* **1882**, *41*, 202–209.
[27] E. Larsen, W. A. Cilley, *J. Inorg. Nucl. Chem.* **1968**, *30*, 287–293.
[28] K. Varshney, M. Rafiquee, A. Somya, *Colloids Surf. A* **2007**, *301*, 69–70.
[29] T. Parangia, B. Wanib, U. Chudasama, *Electrochim. Acta* **2014**, *148*, 79–84.
[30] T. O. Shekunova, A. E. Baranchikov, O. S. Ivanova, L. S. Skogareva, N. P. Simonenko, Yu. A. Karavanova, V. A. Lebedev, L. P. Borilo, V. K. Ivanov, *J. Non-Cryst. Solids* **2016**, *447*, 183–189.
[31] V. Favre-Nicolin, R. J. Cerny, *J. Appl. Crystallogr.* **2002**, *35*, 734–743.
[32] V. Petricek, M. Dusek, L. Palatinus, *Z. Kristallogr.* **2014**, *229*, 345–352.
[33] N. Clavier, R. Podor, N. Dacheux, *J. Eur. Ceram. Soc.* **2011**, *31*, 941–976.
[34] A. I. Orlova, *Radiochemistry* **2002**, *44*, 423–445.
[35] A. I. Orlova in *Structural Chemistry of Inorganic Actinide Compounds* (Eds.: S. V. Krivovichev, P. C. Burns, I. G. Tananaev), Elsevier B. V., Netherlands, **2007**, pp. 315–340.
[36] N. Dacheux, N. Clavier, G. Wallez, V. Brandel, J. Emery, M. Quarton, M. Genet, *Mater. Res. Bull.* **2005**, *40*, 2225–2242.
[37] I. Iglesias, B. F. Alfonso, Z. Amghouz, C. Trobajo, J. R. García, J. A. Huidobro, *Ceram. Int.* **2017**, *43*, 10776–10783.
[38] D. Qin, C. Gausse, S. Szenknect, A. Mesbah, N. Clavier, N. Dacheux, *J. Chem. Thermodyn.* **2017**, *114*, 151–164.
[39] R. D. Shannon, C. T. Prewitt, *Acta Crystallogr., Sect. B: Struct. Sci.* **1969**, *25*, 925–946.
[40] M. A. Salvado, P. Pertierra, A. I. Bortun, C. Trobajo, J. R. Garcıa, *Inorg. Chem.* **2008**, *47*, 7207–7210.
[41] A. Clearfield, B. D. Roberts, M. A. Subramanlan, *Mater. Res. Bull.* **1984**, *19*, 219–226.
[42] A. I. Orlova, V. Yu. Volgutov, G. R. Castro, S. García-Granda, S. A. Khainakov, J. R. García, *Inorg. Chem.* **2009**, *48*, 9046–9047.
[43] L. Troost, L. Ouvrard, *Ann. Chim. Phys.* **1889**, *17*, 227–245.
[44] V. Sidey, *Acta Crystallogr., Sect. B: Struct. Sci.* **2016**, *72*, 626–633.
[45] K. Wang, J. Zhang, J. Wang, C. Fang, W. Yu, X. Zhao, H. Xu, *J. Appl. Crystallogr.* **2005**, *38*, 675–677.
[46] Z. Khadraoui, K. Horchani-Naifer, M. Ferhi, M. Ferid, *Opt. Mater.* **2015**, *47*, 484–489.
[47] Z. Zhang, J. Shi, X. Wang, S. Liu, X. Wang, *J. Rare Earths* **2016**, *34*, 1103–1110.
[48] P. Savchyn, I. Karbovnyk, V. Vistovskyy, A. Voloshinovskii, V. Pankratov, M. Cestelli Guidi, C. Mirri, O. Myahkota, A. Riabtseva, N. Mitina, A. Zaichenko, A. I. Popov, *J. Appl. Phys.* **2012**, *112*, 124309.

[49] S. Petit, D. Righi, A. Decarreau, J. Madejová, *Clay Miner.* **1999**, *34*, 543–549.
[50] S. Petit, D. Righi, J. Madejová, *Appl. Clay Sci.* **2006**, *34*, 22–30.
[51] J. T. Kloprogge, M. Broekmans, L. V. Duong, W. N. Martens, L. Hickey, R. L. Frost, *J. Mater. Sci.* **2006**, *41*, 3535–3539.
[52] A. Hadrich, A. Lautié, T. Mhiri, F. Romain, *Vib. Spectrosc.* **2001**, *26*, 51–64.
[53] V. S. Kurazhkovskaya, D. M. Bykov, A. I. Orlova, *J. Struct. Chem.* **2004**, *45*, 966–973.
[54] M. Nazaraly, G. Wallez, C. Chaneac, E. Tronc, F. Ribot, M. Quarton, J.-P. Jolivet, *J. Phys. Chem. Solids* **2006**, *67*, 1075–1078.
[55] L. S. Skogareva, T. O. Shekunova, A. E. Baranchikov, A. D. Yapryntsev, A. A. Sadovnikov, M. A. Ryumin, N. A. Minaeva, V. K. Ivanov, *Russ. J. Inorg. Chem.* **2016**, *61*, 1219–1224.
[56] N. Dacheux, R. Podor, V. Brandel, M. Genet, *J. Nucl. Mater.* **1998**, *252*, 179–186.
[57] C. E. Bamberger, G. M. Begun, J. Brynestad, J. F. Land, *Radiochim. Acta* **1982**, *31*, 57–64.
[58] I. L. von Botto, E. J. Baran, *Z. Anorg. Allg. Chem.* **1977**, *430*, 283–288.
[59] T. Oi, K. Horio, R. Kikuchi, H. Takahashi, *J. Therm. Anal. Calorim.* **2001**, *65*, 305–308.
[60] V. K. Ivanov, A. E. Baranchikov, O. S. Polezhaeva, G. P. Kopitsa, Yu. D. Tret'yakov, *Russ. J. Inorg. Chem.* **2010**, *55*, 325–327.

Received: September 27, 2018

Rare-Earth Phosphates

Crystallization Pathways of Cerium(IV) Phosphates Under Hydrothermal Conditions: A Search for New Phases with a Tunnel Structure

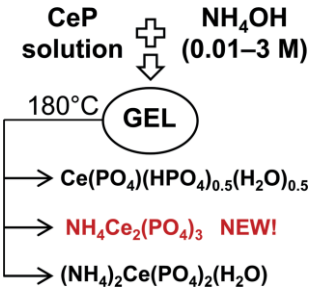

A selective hydrothermal synthesis was proposed for crystalline ceric phosphates $Ce(PO_4)(HPO_4)_{0.5}(H_2O)_{0.5}$, $(NH_4)_2Ce(PO_4)_2(H_2O)$, and previously unknown $NH_4Ce_2(PO_4)_3$.

DOI: 10.1002/ejic.201801182